Quasielastic and inelastic inclusive electron scattering by nuclear systems: Nucleon momentum distributions, spectral functions, and off-shell effects

C. Ciofi degli Atti
Dipartimento di Fisica, Universitá di Perugia, Via A. Pascoli, I-06100 Perugia, Italy
and Istituto Nazionale di Fisica Nucleare, Sezione Sanitá, Viale Regina Elena 299, I-00161, Roma, Italy

D. B. Day
Institute of Nuclear and Particle Physics and Department of Physics, University of Virginia, Charlottesville, Virginia 22901

S. Liuti*
Institute of Nuclear and Particle Physics and Department of Physics, University of Virginia, Charlottesville, Virginia 22901
(Received 3 December 1991)

Inclusive quasielastic and inelastic scattering from nuclei and nuclear matter is analyzed within the plane wave impulse approximation. Theoretical results obtained using model spectral functions including the effects from nucleon-nucleon correlations are presented and compared with results obtained with realistic many-body spectral functions for ^{3}He and nuclear matter. The sensitivity of quasielastic and inelastic nuclear structure functions to different prescriptions for the off-shell behavior of nucleons is investigated in both the $x<1$ and $x>1$ kinematic regions. Results indicate that the inelastic scattering in the $x>1$ region will only be important at momentum transfers above 8 $(\mathrm{GeV}/c)^2$.

PACS number(s): 25.30.Fj

I. INTRODUCTION

Inclusive electron scattering off nuclei represents a powerful tool for investigating the effective constituents of hadronic matter and their dynamics (see, e.g., [1]). As a matter of fact, experiments performed in different regions of the four-momentum (Q^2) and energy (ν) transfers, can provide unique information on different constituents of nuclei: (i) in the region of *quasielastic scattering* ($\nu \leq Q^2/2M_N$, M_N is the nucleon mass), an analysis of the experimental data in terms of y scaling (see, e.g., [2] and [3]) provides information on nucleon dynamics in the hadronic medium, in particular on nucleon momentum distributions [3]; (ii) in the region of *inelastic scattering* ($\nu \geq Q^2/2M_N + M_\pi$, M_π is the pion mass), nucleon resonances are excited allowing a study of how the nuclear medium modifies their properties; (iii) in the region of *deep inelastic scattering* [$W>2$ GeV, $Q^2>1$ $(\mathrm{GeV}/c)^2$, W being the invariant mass of the final hadronic state] possible modifications of the quark and gluon distributions induced by the nuclear medium can in principle be investigated [4]. These three regions are never completely separated one from each other, and the possibility that one or more processes contribute in the kinematic region where one particular process is expected to be dominant, has always to be carefully considered. Typical cases, in this respect, are the inelastic contributions in the region of y scaling, where quasielastic scattering from nucleons is expected to be the leading process and, conversely, the quasielastic contributions in the deep inelastic region, particularly at high W and for values of the Bjorken variable $x = Q^2/2M_N\nu$ greater than 1. It is therefore necessary to have under control a theoretical treatment of the inclusive cross section in the whole range of momentum and energy transfer, so that the contributions from various processes can be clearly identified. To this end, a careful treatment of nuclear structure effects is a prerequisite, which means that the energy and momentum distributions of nucleons have to be taken into account through the use of realistic spectral functions. It is the aim of this paper to present a thorough theoretical treatment of quasielastic and inelastic inclusive cross sections and compare them with available experimental data for few-body systems, complex nuclei and nuclear matter. The main points which will be considered in our paper concern the following: (1) the treatment of nuclear structure in terms of spectral functions characterized by the momentum and removal energy distributions which are generated by nucleon-nucleon correlations; (2) a comparison of such a treatment with the commonly used Fermi smearing procedure, in which nuclear effects are taken into account only in terms of nucleon momentum distributions, i.e., by disregarding nucleon binding effects; and (3) the effects of various off-shell extrapolations of the free nucleon structure functions on the inclusive electron-nucleus cross section.

Our paper is organized as follows. In Sec. II the general structure of the inclusive cross section in plane wave impulse approximation (PWIA) is discussed, paying particular attention to off-shell effects, current conservation, and the nucleon spectral function; various forms of the

*Permanent address: INFN, Sezione Sanita', Viale Regina Elena 299, I-00161, Roma, Italy.

quasielastic and inelastic cross sections, corresponding to different off-shell prescriptions are given in Sec. III; the comparison between theoretical calculations and experimental data is presented in Sec. IV; the effects of inelastic contributions on the y-scaling analysis of data in the $x > 1$ region are shown in Sec. V, and the effects of quasielastic scattering on the extraction of deep inelastic nuclear structure functions at $x > 1$, are illustrated in Sec. VI. A summary and our conclusions are presented in Sec. VII.

II. INCLUSIVE ELECTRON-NUCLEUS SCATTERING IN PLANE WAVE IMPULSE APPROXIMATION

A. The nuclear response

The inclusive cross section for electron scattering by a nucleus A in first Born approximation, depicted in Fig. 1, is given in the laboratory system by the following expression (see Appendix A):

$$\frac{d^2\sigma}{d\Omega_{e'}d\epsilon_2}=\sigma_{\rm Mott}\left[\left[\frac{Q^2}{|\mathbf{q}|^2}\right]^2 R_L^A(Q^2,W)+\left[\frac{1}{2}\frac{Q^2}{|\mathbf{q}|^2}+\tan^2\frac{\theta}{2}\right]R_T^A(Q^2,W)\right] \tag{1}$$

$$=\sigma_{\rm Mott}\left[W_2^A(Q^2,W)+2\tan^2\frac{\theta}{2}W_1^A(Q^2,W)\right], \tag{2}$$

where $\sigma_{\rm Mott}=\alpha^2\cos^2(\theta/2)/4\epsilon_1^2\sin^4(\theta/2)$ is the Mott cross section, $Q^2=-q^2=\mathbf{q}^2-\nu^2=4\epsilon_1\epsilon_2\sin^2(\theta/2)>0$ is the squared four-momentum transfer, θ is the scattering angle, and $W^2=(P_A+q)^2=M_A^2+2M_A\nu-Q^2$ is the invariant mass of the nucleus [in this paper a four-vector is denoted by $a\equiv(a_0,\mathbf{a})$ and $a^2=a_0^2-\mathbf{a}^2$]. The relation between the longitudinal (R_L^A) and transverse (R_T^A) response functions and the response functions W_1^A and W_2^A, which we adopt in this paper, is

$$W_1^A(Q^2,W)=\tfrac{1}{2}R_T^A(Q^2,W)\ , \tag{3}$$

$$W_2^A(Q^2,W)=\left[\frac{Q^2}{|\mathbf{q}|^2}\right]^2 R_L^A(Q^2,W)+\frac{1}{2}\frac{Q^2}{|\mathbf{q}|^2}R_T^A(Q^2,W)\ . \tag{4}$$

The explicit evaluation of the response functions W_1^A and W_2^A within microscopic nuclear structure requires a model for both the hadronic current and the initial and final nuclear states. The plane wave impulse approximation (PWIA), which is depicted in Fig. 2, is used throughout. The four-momenta of the initial nucleus A, of the bound off-shell nucleon N, of the final nucleon state $A-1$ and of the final hadronic state X, are

$$P_A\equiv(M_A,0)\ , \tag{5}$$

$$P_{A-1}\equiv((\mathbf{p}^2+M_{A-1}^{*2})^{1/2},-\mathbf{p})\ , \tag{6}$$

$$p\equiv(p_0,\mathbf{p})\ , \tag{7}$$

$$p_X\equiv((\mathbf{p}X^2+M_X^2)^{1/2},\mathbf{p}_X)\ , \tag{8}$$

where $\mathbf{p}_X=\mathbf{p}+\mathbf{q}$ and $M_{A-1}^*=M_{A-1}+E_{A-1}^{f*}$. M_{A-1}^* and E_{A-1}^{f*} are the mass and intrinsic excitation energy of the final $(A-1)$-nucleon state, respectively. The PWIA allows one to express the nuclear responses $W_{1(2)}^A$ in terms of a convolution integral involving the nucleon spectral function $P^N(\mathbf{p},E)$ (representing the joint probability of finding in the target nucleus a nucleon with momentum $\mathbf{p}$ and removal energy $E=M_{A-1}^*+M_N-M_A$), and the electromagnetic response functions $W_{1(2)}^{N,\rm off}$ for an off-shell

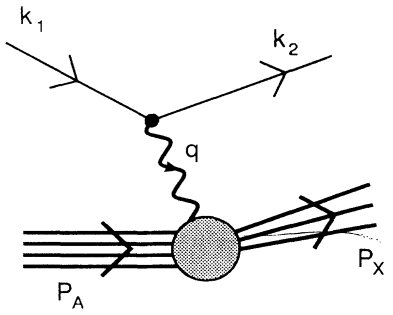

FIG. 1. Inclusive electron-nucleus scattering diagram in the one photon-exchange approximation. $k_{1(2)}\equiv(\mathbf{p}_{1(2)},\epsilon_{1(2)})$ represents the initial (final) electron four-momentum, $q\equiv(\nu,\mathbf{q})\equiv k_1-k_2$ $(Q^2=-q^2=\mathbf{q}^2-\nu^2)$, the four-momentum transfer, and $P_A\equiv(M_A,0)$ and P_X the four-momenta of the initial and final nuclear systems, respectively.

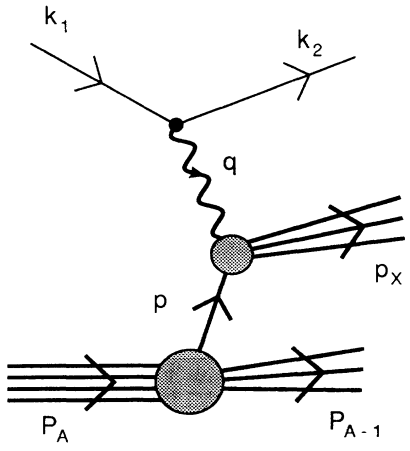

FIG. 2. Impulse approximation diagram for electron scattering off nuclei. The four-momenta in the laboratory system are $P_A\equiv(M_A,0)$, $P_{A-1}\equiv((\mathbf{p}^2+M_{A-1}^{*2})^{1/2},-\mathbf{p})$, $p\equiv(M_A-(\mathbf{p}^2+M_{A-1}^{*2})^{1/2},\mathbf{p})$, and $p_X\equiv((\mathbf{p}_X^2+M_X^2)^{1/2},\mathbf{p}_X)$ and refer to the initial nucleus A, to the recoiling final $A-1$ system, to the struck nucleon, and to the final hadronic system at the nucleon vertex, respectively.

nucleon. However, it is well known that the PWIA, based on the assumption that the nucleon current is the sum of single nucleon currents, does not satisfy current conservation; moreover, there are many ways the free nucleon structure functions can be extrapolated off-shell. As a result, the nuclear response functions do not have a unique form. Their general form can be written in the following way (see Appendix B):

$$W^A_{1(2)}(Q^2,W)=\int d\mathbf{p}\int dE Z P^p(|\mathbf{p}|,E)[C_{1(2)}W_1^{p,\text{off}}(\tilde{Q}^2,\tilde{W},p^2)+D_{i(2)}W_2^{p,\text{off}}(\tilde{Q}^2,\tilde{W},p^2)]$$
$$+(\text{similar terms for the neutrons}) , \tag{9}$$

where Z is the number of protons, $W^{N,\text{off}}_{1(2)}$ $(N=p,n)$ are the off-shell nucleon structure functions, $\tilde{Q}^2$ is the squared four-momentum transfer, $\tilde{W}$ is the invariant mass of the knocked-out hadron, and p^2 is the four-momentum squared of the struck nucleon. $C_{1(2)}$ and $D_{1(2)}$ are kinematic factors whose explicit form depends on the way the off-shell nucleon is treated and, finally, $P^N(|\mathbf{p}|,E)$ is the nucleon spectral function. From Eq. (9) it can be seen that two basic ingredients are necessary in order to calculate the nuclear response $W^A_{1(2)}$: the nucleon spectral function $P^N(|\mathbf{p}|,E)$ and the off-shell nucleon responses $W^{N,\text{off}}_{1(2)}$. For both quantities a practical choice has to be made, for, as is well known, realistic spectral functions exist to date only for $A=3$ [6–8] and nuclear matter, [9] and, in addition, several prescriptions for the off-shell extrapolation of the nucleon response can be adopted (see next section).

B. Off-shell extrapolations and current conservation prescriptions

In this paper we follow three different prescriptions to treat off-shell effects and current conservation: (a) the prescription of [10], initially introduced to treat inelastic and deep inelastic channels, and extended here to quasi-elastic (q.e.) channels, according to which

$$p\equiv(M_A-(\mathbf{p}^2+M^{*2}_{A-1})^{1/2},\mathbf{p}) , \tag{10a}$$
$$\tilde{Q}^2=Q^2=-q^2=\mathbf{q}^2-\nu^2 , \tag{10b}$$
$$\tilde{W}^2=(p+q)^2 , \tag{10c}$$
$$W^{N,\text{off}}_{1(2)}(\tilde{Q}^2,\tilde{W},p^2)=W^{N,\text{on}}_{1(2)}(Q^2,\tilde{W}) ; \tag{10d}$$

(b) the same prescription as in (a) but with current conservation enforced by taking for the time-transverse components of $W^{N,\text{off}}_{\mu\nu}$ the same form as for the free nucleon hadronic tensor $W^N_{\mu\nu}$, and by determining the longitudinal ones from the condition

$$q_\mu W^{N,\text{off}}_{\mu\nu}=W^{N,\text{off}}_{\mu\nu}q_\nu=0 ; \tag{11}$$

(c) the prescription of [11] which was introduced to treat quasi-elastic channels, extended here to inelastic and deep inelastic channels. In this prescription the bound nucleon interacting with the virtual photon is considered to be on-shell and current conservation is enforced as in prescription (b):

$$p\equiv\bar{p}=((M_N^2+\mathbf{p}^2)^{1/2},\mathbf{p}) , \tag{12a}$$
$$\tilde{Q}^2=\bar{Q}^2=-\bar{q}^2=\mathbf{q}^2-\bar{\nu}^2 , \tag{12b}$$
$$\bar{\nu}=\nu-(M_N^2+\mathbf{p}^2)^{1/2}+M_A-(\mathbf{p}^2+M^{*2}_{A-1})^{1/2} , \tag{12c}$$
$$\tilde{W}^2=(\bar{p}+\bar{q})^2=(p+q)^2 , \tag{12d}$$
$$W^{N,\text{off}}_{1(2)}(\tilde{Q}^2,\tilde{W},p^2)=W^{N,\text{on}}_{1(2)}(\bar{Q}^2,\tilde{W}) . \tag{12e}$$

It is worth pointing out that the three prescriptions have in common the following features: (i) The off-shell nucleon structure functions do not include dynamical modifications and, therefore, they are assumed to have the same form as the free ones [cf. Eqs. (10d) and (12e)], without any further dependence upon the invariant p^2. (ii) Both the invariant mass, $\tilde{W}$, and the component $p_\parallel\equiv(\mathbf{p}\cdot\mathbf{q})/|\mathbf{q}|$ of the off-shell nucleon are the same [cf. Eqs. (10c) and (12d)] so that the mapping of the off-shell to the on-shell structure functions is carried out unambiguously in all prescriptions. In addition, no ambiguity is introduced in the treatment of the energy conserving δ function which appears in the q.e. cross section (see Sec. III), thus implying that off-shell effects do not affect the analysis of such cross sections in terms of y scaling (see Sec. V).

C. The nucleon spectral function and momentum distributions

The nucleon spectral function $P^N(|\mathbf{p}|,E)$ appearing in Eq. (9) represents the joint probability of finding in the target nucleus a nucleon with momentum $|\mathbf{p}|$ and removal energy E or, equivalently, the joint probability distribution that, after a nucleon with momentum $|\mathbf{p}|$ has been removed from the target, the $(A-1)$ system is left with excitation energy E^{f*}_{A-1}. By disregarding, only for ease of presentation, any difference between the proton and the neutron spectral function, $P^N(|\mathbf{p}|,E)$ can be defined as follows (cf. Appendix B) [12]:

$$P^N(|\mathbf{p}|,E)=\frac{1}{2J+1}\sum_{M,\sigma}\langle\Psi^{JM}_A|a^\dagger_{\mathbf{p},\sigma}\delta(E-(\hat{H}_{A-1}-E_A))a_{\mathbf{p},\sigma}|\Psi^{JM}_A\rangle , \tag{13a}$$
$$=\frac{1}{2J+1}\sum_{M,\sigma}\sum_f|\langle\Psi^f_{A-1}|a_{\mathbf{p},\sigma}|\Psi^{JM}_A\rangle|^2\delta(E-(E^f_{A-1}-E_A)) , \tag{13b}$$
$$=\frac{1}{2J+1}(2\pi)^{-3}\sum_{M,\sigma}\sum_f\left|\int d\mathbf{z}\,e^{i\mathbf{p}\cdot\mathbf{z}}G^{M,\sigma}_f(\mathbf{z})\right|^2\delta(E-(E^f_{A-1}-E_A)) , \tag{13c}$$

where $a^{\dagger}_{\mathbf{p},\sigma}$ ($a_{\mathbf{p},\sigma}$) is the creation (annihilation) operator of a nucleon with momentum $\mathbf{p}$ and spin σ, $\hat{H}_{A-1}$ the intrinsic Hamiltonian for the $A-1$ interacting nucleons, and Ψ^{JM}_A the eigenfunction of the ground state of the Hamiltonian for the A-nucleon system (with eigenvalue E_A, total angular momentum J, and third component M). The function $G_f^{M,\sigma}(\mathbf{z})$ in Eq. (13c) is the overlap integral

$$G_f^{M,\sigma}(\mathbf{z}) = \langle \chi_\sigma^{1/2}, \Psi^f_{A-1}(\mathbf{x}_{1,\ldots,}\mathbf{x}_{A-1}) | \Psi^{JM}_A(\mathbf{x}_1,\ldots,\mathbf{x}_{A-1},\mathbf{z}) \rangle \tag{14}$$

between the eigenfunction Ψ^{JM}_A and the eigenfunction Ψ^f_{A-1} (with eigenvalue $E^f_{A-1}=E_{A-1}+E^{f*}_{A-1}$) of the state f of the intrinsic Hamiltonian $\hat{H}_{A-1}$ pertaining to the system of $A-1$ interacting nucleons, $\chi^{1/2}_\sigma$ representing a spin wave function. Since the set of states f includes also continuum states of the residual $A-1$ system, the sum over f in Eq. (13) stands for a sum over the discrete states of the $A-1$ system and an integration over the continuum states. The spectral function, which is normalized according to

$$\int P^N(|\mathbf{p}|,E)d\mathbf{p}\,dE = 1 , \tag{15}$$

can be represented in the general form [7,9]

$$P^N(|\mathbf{p}|,E) = P^N_{\rm gr}(|\mathbf{p}|,E) + P^N_{\rm ex}(|\mathbf{p}|,E) , \tag{16}$$

where $P^N_{\rm gr}(|\mathbf{p}|,E)=n_{\rm gr}(|\mathbf{p}|)\delta(E-E_{\rm min})$ yields the probability distribution that the final $A-1$ system is left in its ground state (corresponding to $E^{f*}_{A-1}=0$ and $E=E_{\rm min}=M_{A-1}+M_N-M_A$), whereas $P^N_{\rm ex}(|\mathbf{p}|,E)$ yields the probability distribution that the final $A-1$ system is left in an excited state with excitation energy $E^{f*}_{A-1}=E-E_{\rm min}$. The exact relations between the spectral function and the momentum distribution will be used in what follows

$$n(|\mathbf{p}|) = (2\pi)^{-3}\int e^{i\mathbf{p}\cdot(\mathbf{z}-\mathbf{z}')}\rho(\mathbf{z},\mathbf{z}')d\mathbf{z}\,d\mathbf{z}' = \int_{E_{\rm min}}^{\infty} P^N(|\mathbf{p}|,E)dE , \tag{17}$$

where $\rho(\mathbf{z},\mathbf{z}')$ is the nondiagonal one-body density matrix. Eq. (16) holds for any value of A but for a complex nucleus it is also useful to adopt another representation of the spectral function in which the ground state of the $A-1$ system and its excited states represented by one-hole excitations are explicitly separated out from more complex configurations, e.g., one-particle–two-hole states, which can be reached when two-particle–two-hole states in the target nucleus are considered. One has [13]

$$P^N(|\mathbf{p}|,E) = P^N_0(|\mathbf{p}|,E) + P^N_1(|\mathbf{p}|,E) , \tag{18}$$

with

$$P^N_0(|\mathbf{p}|,E) = \frac{1}{2J+1}(2\pi)^{-3}\sum_{M,\sigma}\sum_{\alpha}\left|\int d\mathbf{z}\,e^{i\mathbf{p}\cdot\mathbf{z}}G^{M,\sigma}_\alpha(\mathbf{z})\right|^2\delta(E-|\epsilon_\alpha|) = \sum_\alpha \frac{A_\alpha}{A}n_\alpha(|\mathbf{p}|)\delta(E-|\epsilon_\alpha|) , \tag{19}$$

$$P^N_1(|\mathbf{p}|,E) = \frac{1}{2J+1}(2\pi)^{-3}\sum_{M,\sigma}\sum_{f\neq\alpha}\left|\int d\mathbf{z}\,e^{i\mathbf{p}\cdot\mathbf{z}}G^{M,\sigma}_f(\mathbf{z})\right|^2\delta(E-E^f_1) , \tag{20}$$

where $n_\alpha(|\mathbf{p}|)$ is the hole state momentum distribution with single particle (s.p.) energy ϵ_α and nucleon number A_α ($\sum_\alpha A_\alpha = A$), the sum over α runs only over hole states of the target, and $E^f_1 \equiv E^{f*}_{A-1}+E_{\rm min}$. Within the Hartree-Fock (HF) approximation, $P^N_1(|\mathbf{p}|,E)=0$, and the HF spectral function, viz.

$$P^N_{\rm HF}(|\mathbf{p}|,E) = \sum_\alpha \frac{A_\alpha}{A}n^{\rm HF}_\alpha(|\mathbf{p}|)\delta(E-|\epsilon_\alpha|) , \tag{21}$$

is recovered. The main difference between $n_\alpha(|\mathbf{p}|)$ appearing in Eq. (19) and $n^{\rm HF}_\alpha(|\mathbf{p}|)$, concerns their normalization, or hole state occupation probability; $S_\alpha = \int n_\alpha(|\mathbf{p}|)d\mathbf{p}$ and $S^{\rm HF}_\alpha = \int n^{\rm HF}_\alpha(|\mathbf{p}|)d\mathbf{p}$, respectively; in fact, due to ground-state correlations, $S_\alpha < 1$, whereas $S^{\rm HF}_\alpha = 1$; correspondingly, for a particle state i, $S_i > 0$ and $S^{\rm HF}_i = 0$. For an extended system like nuclear matter, the hole part of the spectral function can be cast in the following form [9]:

$$P^N_0(|\mathbf{p}|,E) = \frac{3}{4\pi p_F^3}Z(|\mathbf{p}|)\Theta(p_F-|\mathbf{p}|)\delta(E+e(|\mathbf{p}|)) , \tag{22}$$

where $Z(|\mathbf{p}|)$ is the hole strength, $e(|\mathbf{p}|)$ is the hole single-particle spectrum, and p_F is the Fermi momentum [in absence of nucleon-nucleon (NN) correlations $e(|\mathbf{p}|)=p^2/2M_N$, $Z(|\mathbf{p}|)=1$ and the usual Fermi gas spectral function is recovered]. It should be pointed out that in Eq. (19) the finite width of the hole states generated by NN correlations has been disregarded; such an approximation has minor effects on the inclusive cross section we are interested in (see Sec. IV B and [14]). It is clear from the very definition of the spectral function [Eq. (13)] that its evaluation implies the knowledge of the whole spectrum of continuum and excited states of the $A-1$ nucleon system. It is for this reason that $P^N(|\mathbf{p}|,E)$ has been calculated to date only for ^{3}He [6–8] and for nuclear matter [9]. In this paper we use for the three-body system a spectral function obtained in [7] within the variational approach, whereas model spectral functions proposed in [14] and [15] are adopted for complex nuclei and nuclear matter, respectively. Such spectral functions are of the form given by Eq. (18) with $P^N_1(|\mathbf{p}|,E)$ obtained [15] from an extended version of the two-nucleon correlation model of [5]. The main feature of $P^N_1(|\mathbf{p}|,E)$ is the presence of high momentum and high

removal energy components generated by two-nucleon correlations. Its explicit calculation performed in [15] for three-body systems and nuclear matter shows a very good agreement with the corresponding microscopic realistic spectral functions [7,9]. Such an agreement in the case of [9] indicates that the modeling of three-body breakup processes associated with two-hole–one-particle intermediate states [9] by means of the two-nucleon correlation mechanism [5] yields a reliable representation for $P_1^N(|\mathbf{p}|,E)$.

III. THE QUASIELASTIC AND INELASTIC CROSS SECTIONS AND THE OFF-SHELL PRESCRIPTIONS

The inclusive elastic and inelastic cross sections will be written in the following form:

$$\left[\frac{d^2\sigma}{d\Omega d\epsilon_2}\right]_i=\sigma_{\text{Mott}}\left[W_2^{A,i}(Q^2,W)+2\tan^2\frac{\theta}{2}W_1^{A,i}(Q^2,W)\right], \tag{23}$$

where i refers to "quasielastic" or "inelastic and deep inelastic" and

$$W_{1(2)}^{A,i}(Q^2,W)=\int d\mathbf{p}\int dE\, ZP^p(|\mathbf{p}|,E)[C_{1(2)}W_1^{p,i}(\tilde{Q}^2,\tilde{W},p^2)+D_{1(2)}W_2^{p,i}(\tilde{Q}^2,\tilde{W},p^2)]$$
$$+(\text{similar terms for neutrons}) . \tag{24}$$

In Eq. (24) (where we used the notation $W^{N,\text{off},i}\equiv W^{N,i}$) the coefficients $C_{1(2)}$ and $D_{1(2)}$ are the same for quasielastic (q.e.) and inelastic scattering and take the following form, depending upon the off-shell and current conservation prescriptions:

$$C_1=1,\quad D_1=\frac{\mathbf{p}^2-p_\parallel^2}{2M_N^2} , \tag{25a}$$

$$C_2=0,\quad D_2=\left[1+\frac{p_\parallel Q^2}{(pq)|\mathbf{q}|}\right]^2\left[\frac{pq}{M_N\nu}\right]^2+\frac{\mathbf{p}^2-p_\parallel^2}{2M_N^2}\frac{Q^2}{|\mathbf{q}|^2} , \tag{25b}$$

with $p_\parallel=\mathbf{p}\cdot\mathbf{q}/|\mathbf{q}|$, in prescription (a);

$$C_1=1,\quad D_1=\frac{\mathbf{p}^2-p_\parallel^2}{2M_N^2} , \tag{26a}$$

$$C_2=\frac{Q^4}{|\mathbf{q}|^4}\frac{M_N^2-p^2}{(pq)},\quad D_2=\left[1+\frac{p_\parallel Q^2}{(pq)|\mathbf{q}|}\right]^2\left[\frac{pq}{M_N\nu}\right]^2+\frac{\mathbf{p}^2-p_\parallel^2}{2M_N^2}\frac{Q^2}{|\mathbf{q}|^2} , \tag{26b}$$

in prescription (b);

$$C_1=1,\quad D_1=\frac{\mathbf{p}^2-p_\parallel^2}{2M_N^2} , \tag{27a}$$

$$C_2=\frac{Q^2}{|\mathbf{q}|^2}\left[1-\frac{Q^2}{\bar{Q}^2}\right],\quad D_2=\left[1+\frac{p_\parallel\bar{Q}^2}{(\bar{p}\,\bar{q})|\mathbf{q}|}\right]^2\left[\frac{\bar{p}\,\bar{q}}{M_N\bar{\nu}}\right]^2+\frac{\mathbf{p}^2-p_\parallel^2}{2M_N^2}\frac{Q^2}{|\mathbf{q}|^2} , \tag{27b}$$

in prescription (c). The difference between q.e. and inelastic scattering is given only by the form of the nucleon structure functions $W_{1(2)}^{N,i}$. For q.e. scattering [the final hadronic state $|X\rangle=|N\rangle$ is a nucleon in its ground state with four-momentum $p_N\equiv((\mathbf{p}_N^2+M_N^2)^{1/2},\mathbf{p}_N)$ with $\mathbf{p}_N=\mathbf{p}+\mathbf{q}$] one has

$$W_1^{N,\text{q.e.}}(\tilde{Q}^2,\tilde{W})=\frac{\tilde{Q}^2}{4M_N^2}[F_1(\tilde{Q}^2)+\kappa F_2(\tilde{Q}^2)]^2\frac{M_N}{E_p}\frac{M_N}{E_p'}\delta(E_p+\nu-E_p') , \tag{28a}$$

$$W_2^{N,\text{q.e.}}(\tilde{Q}^2,\tilde{W})=\left[F_1^2(\tilde{Q}^2)+\kappa^2\frac{\tilde{Q}^2}{4M_N^2}F_2^2(\tilde{Q}^2)\right]\frac{M_N}{E_p}\frac{M_N}{E_p'}\delta(E_p+\nu-E_p') , \tag{28b}$$

where $F_{1,2}$ are the elastic electron-nucleon form factors corresponding to a given parametrization (in our numerical calculations the one in [16] has been used); $E_p=p_0$ and $E_p'=[(\mathbf{p}+\mathbf{q})^2+M_N^2]^{1/2}$ [note that $(M_N/E_p')\delta(E_p+\nu-E_p')$ is equivalent to $2M_N\delta(\tilde{W}^2-M_N^2)$]. In case of inelastic (the final hadronic state $|X\rangle=|N^*\rangle$ represents a nucleon resonance) or deep inelastic scattering ($|X\rangle$ is a jet of hadrons), both the dependence upon the invariant mass $\tilde{W}$ and the momentum transfer $\tilde{Q}^2$ of the nucleon structure functions are usually parametrized to fit the experimental data. In this paper the parametrization of [10], which is given in both the resonance and deep inelastic regions, has been adopted. If prescription (c) is used, it is worthwhile writing the cross section for q.e. scattering in the frequently used form

$$\left[\frac{d^2\sigma}{d\Omega d\epsilon_2}\right]_{\text{q.e.}} = \int dE \int d\mathbf{p}\, P^N(|\mathbf{p}|,E)(Z\sigma_{ep}(|\mathbf{q}|,\nu,|\mathbf{p}|,E)+N\sigma_{\text{en}}(|\mathbf{q}|,\nu,|\mathbf{p}|,E))\delta(\nu+M_A-E'_p-(P_{A-1})_0)\ , \tag{29}$$

where and $\sigma_{eN}(|\mathbf{q}|,\nu,|\mathbf{p}|,E)$ is the electron-nucleon cross section (without the flux factor) for scattering by an off-shell nucleon with momentum $\mathbf{p}$, i.e., [11],

$$\sigma_{eN}(|\mathbf{q}|,\nu,|\mathbf{p}|,E)=\frac{\sigma_{\text{Mott}}}{E_pE'_p}\left\{\frac{Q^4}{|\mathbf{q}|^4}\left[\frac{(E_p+E'_p)^2}{4}(F_1^2+\bar{\tau}\kappa^2F_2^2)-\frac{|\mathbf{q}|^2}{4}(F_1+\kappa F_2)^2\right]\right.$$
$$\left.+\left[\tan^2\frac{\theta}{2}+\frac{Q^2}{2|\mathbf{q}|^2}\right]\left[p_\perp^2(F_1^2+\bar{\tau}\kappa^2F_2^2)+\frac{\bar{Q}^2}{2}(F_1+\kappa F_2)^2\right]\right\}, \tag{30}$$

where the form factors F_1 and F_2 are evaluated at $\tilde{Q}^2=Q^2$ and $\bar{\tau}=\bar{Q}^2/4M_N^2$.

IV. COMPARISON OF THEORETICAL CALCULATIONS WITH EXPERIMENTAL DATA

In this section the theoretical inclusive cross section given by the sum

$$\frac{d^2\sigma}{d\Omega d\epsilon_2}=\left[\frac{d^2\sigma}{d\Omega d\epsilon_2}\right]_{\text{q.e.}}+\left[\frac{d^2\sigma}{d\Omega d\epsilon_2}\right]_{\text{in}} \tag{31}$$

is compared with the experimental data for ^{3}He, ^{4}He, ^{12}C, ^{56}Fe, and nuclear matter, obtained in [17–19] in a wide range of values of momentum and energy transfers.

The aim of such a comparison is to thoroughly analyze how the inclusive quasielastic and inelastic cross sections are affected by nuclear structure and by various types of off-shell extrapolations of the free nucleon structure functions. The results of calculations obtained by using a specific model for both the spectral function and the off-shell prescription are presented in Sec. 4.1; various spectral functions are compared and the effects of nucleon-nucleon correlations are illustrated in Sec. IV B; in Sec. IV C the results obtained with the simple Fermi-motion smearing procedure are shown and, finally, in Sec. IV D the sensitivity of the cross sections to different off-shell prescriptions is analyzed.

A. Results for ^{3}He, ^{4}He, ^{12}C, ^{56}Fe, and nuclear matter and effects of nucleon-nucleon correlations

We calculated the quasielastic and inelastic cross sections according to Eqs. (23) and (24) by using the spectral function (18) and the off-shell prescription (c) [Eqs. (27a) and (27b)]. Such prescription allows us to compare our results with the ones of [20] and [21], where the same treatment of the off-shell nucleon has been adopted for ^{3}He and nuclear matter, respectively. The main ingredients of the spectral function P_0^N are the hole state occupation probabilities, $S_\alpha \equiv S_0$, and the hole energies, ϵ_α (see Sec. II C). In agreement with recent many-body calculations, we adopted the following values for S_α: $S_\alpha=0.80$ for ^{4}He [22,23], ^{12}C [24], and ^{56}Fe [25], $S_\alpha=0.75$ for nuclear matter [9]; the values of the hole energies ϵ_α have been taken from $(e,e'p)$ reactions [26]. As for the evaluation of the spectral function $P_1^N(|\mathbf{p}|,E)$, one essentially needs to know the nucleon momentum distributions and mean removal energies; such quantities have also been taken from many-body calculations (see [14] for details). The results of calculations for ^{3}He, ^{4}He, ^{12}C, ^{56}Fe, and nuclear matter are given in Figs. 3, 4, 5, 6, and 7, respectively. They are presented both on linear and log scales; the former better shows the difference between experimental data and theoretical calculations in the region of the q.e. peak ($\nu\approx\nu_{\text{peak}}$, $x\approx1$) and inelastic channels ($\nu\geq\nu_{\text{peak}}$, $x\leq1$), whereas the latter is better suited to illustrate the region of y scaling ($\nu\leq\nu_{\text{peak}}$, $x\geq1$). An analysis of the results presented in Figs. 3–7 allows one to observe some features which are common for all nuclei considered, viz. the following:

(i) The quasielastic region is fairly well reproduced, except for a systematic discrepancy at low energy transfer, which decreases with increasing momentum transfer; such a discrepancy, most likely, should be ascribed (see e.g., [21,27–29]) to the effects of final state interaction (FSI) between the ejected nucleon and the final $A-1$ system, which is disregarded in the PWIA. (ii) At low momentum transfer, the "dip" region between the quasielastic and inelastic channels is underestimated by an amount which decreases with increasing momentum transfer. (iii) In the region of momentum transfer covered by the present experimental data, the contribution of inelastic channels at low energy transfer is irrelevant, which means that the analysis of the data in terms of y scaling (see [2] and [3]) is well justified. (iv) For ^{3}He and nuclear matter our results are in very good agreement with the ones of [20] and [21], respectively, obtained with many-body spectral functions resulting from accurate solutions of the many-body Schrödinger equation with realistic interactions. This point will be discussed in detail in the next subsection.

The separate contributions of P_0 and P_1 to the quasielastic and inelastic cross sections are shown in Fig. 8 and Fig. 9, in order to better illustrate the effects of NN correlations. It can be seen that the most evident effect of NN correlations is to strongly increase the tails of the PWIA cross sections through the contribution of P_1. In particular, at the highest values of Q^2, the cross section at $\nu<\nu_{\text{peak}}$ ($x>1$) is almost completely exhausted by P_1, both in its quasielastic and inelastic parts. On the contrary, at high Q^2 and $\nu>\nu_{\text{peak}}$ ($x<1$), the inelastic channels become dominant and the cross section is mainly determined by the two-body breakup part of the spectral

function, the three-body breakup part lying at least one order of magnitude below.

B. Comparison between different spectral functions

In this section we present a comparison between results for ^{3}He and nuclear matter obtained with the model spectral function of [15] and with variational spectral functions ([7] and [9], respectively). The main features of the spectral function which govern the behavior of the inclusive cross section in PWIA at high momentum transfer are the following: (i) the value of $\langle 1/k \rangle$ which determines the height of the quasielastic peak; (ii) the two-body breakup contribution to the spectral function,

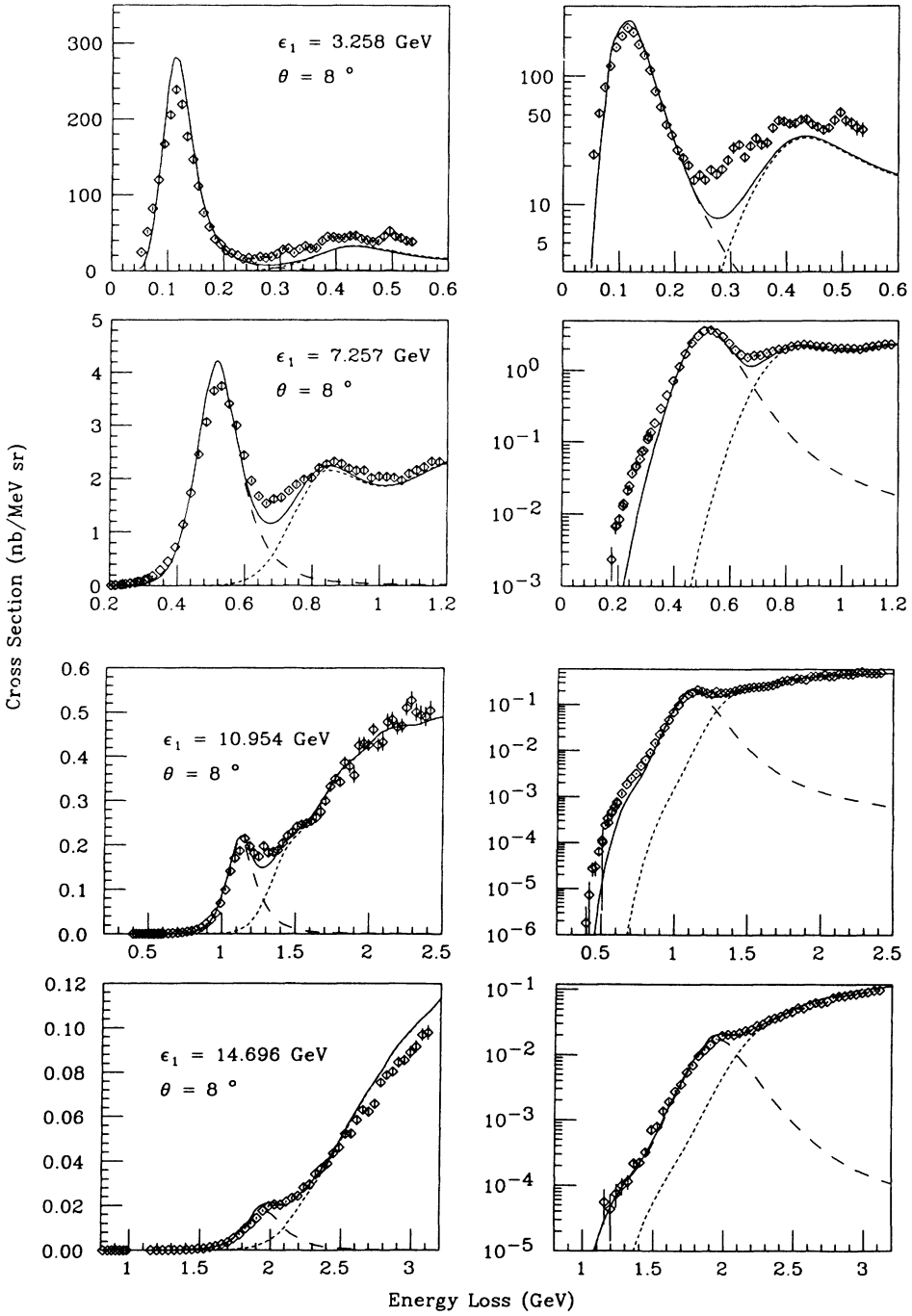

FIG. 3. The inclusive cross section for the process ^{3}He(e,e') at various kinematics shown on linear (left) and log (right) scales versus the energy loss ν. Long dashes: quasielastic contribution; short dashes: inelastic contributions; solid line: total (quasielastic plus inelastic) cross section. The average four-momentum squared corresponding to the various kinematics is $Q^2 \approx 0.2$ GeV^2 at $\epsilon_1 = 3.258$ GeV, $Q^2 \approx 1$ GeV^2 at $\epsilon_1 = 7.257$ GeV, $Q^2 \approx 2$ GeV^2 at $\epsilon_1 = 10.954$ and $Q^2 \approx 3.5$ GeV^2 at $\epsilon_1 = 14.696$ GeV. All curves presented in this figure, as well as in Figs. 4–12, were obtained by using the off-shell prescription (c). Experimental data from [17].

P_0, which determines the region around the peak; and (iii) the three-body breakup part P_1, which governs the region at $\nu \ll \nu_{\text{peak}}$ ($x > 1$).

From Fig. 10, where our results are compared with the variational calculations for ^{3}He [7] and nuclear matter [9], it can be seen that all features listed above are correctly reproduced, in that the model of [15] provides a spectral function which yields almost the same inclusive cross section as the variational ones. As a matter of fact, the spectral function of [15] yields the correct values of $\langle 1/k \rangle$, and it is therefore expected that the height of the peak would be correctly reproduced. As for the two-body breakup contribution, it should be pointed out that the calculation of [9] also includes, with respect to ours, a finite removal energy width for P_0, generated by perturbative corrections to the ground and one-hole states. Although the account for the finite width does indeed produce a change in the shape of the spectral function [9], such an effect is not noticeable in the cross sections for inclusive processes, in the kinematical range considered in this paper ($Q^2 \geq 1$ GeV^2 and ν varying within a few GeV range). This feature is not present when comparing with calculations performed using the spectral function of [7]. Since the spectral function of [15] correctly reproduces the values $\langle E \rangle$, $\langle T \rangle$, as well as the high momentum and high removal energy distributions of many-body spectral functions, it is expected that our calculation in the region dominated by P_1 ($x > 1$) will agree with similar calculations obtained with many-body spectral functions. This is again confirmed by the results in Fig. 10. Finally, in the region $\nu \gg \nu_{\text{peak}}$ and $x < 1$, where the cross section is dominated by inelastic scattering, the detailed correlation structure of the spectral function does not play an important role, due to the fact that all components including the ones below the Fermi level are integrated over in Eq. (9). The kinematics considered in Fig. 10 is such that $Q^2 \simeq 1$ GeV^2 for ^{3}He and $Q^2 \simeq 3$ GeV^2 for nuclear matter; the agreement at other values of the

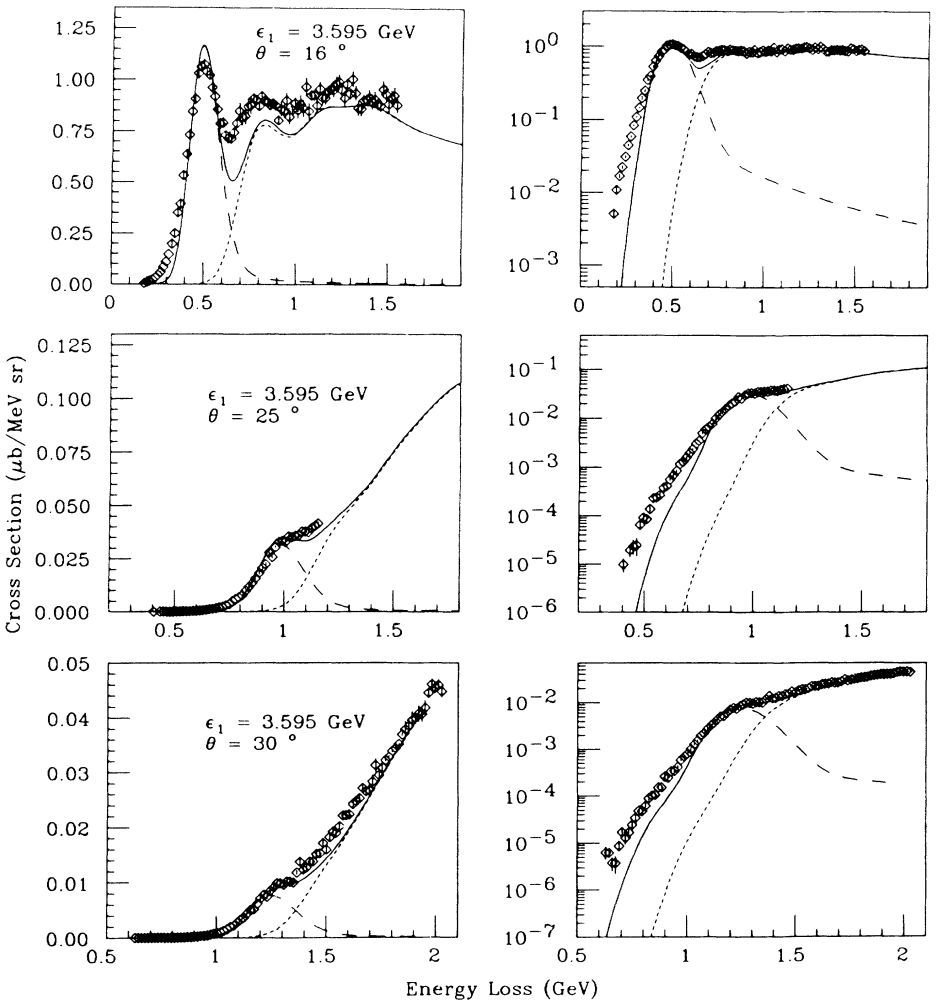

FIG. 4. The same as in Fig. 3 but for ^{4}He. The average square four-momentum transfer is $Q^2 \approx 1$ GeV^2 at $\epsilon_1 = 3.595$ GeV, $\theta = 16°$; $Q^2 \approx 2$ GeV^2 at $\epsilon_1 = 3.595$ GeV, $\theta = 25°$; $Q^2 \approx 3$ GeV^2 at $\epsilon_1 = 3.595$ GeV, $\theta = 30°$. Experimental data from [18].

momentum transfer is of the same quality as the one shown in the figure.

C. The Fermi motion smearing procedure

It was a common practice in the past to take into account nuclear effects by means of the so called Fermi motion smearing procedure (see e.g., [10]), i.e., by using in Eq. (29) only the nucleon momentum distribution $n(|\mathbf{p}|)$ and not the spectral function. In Figs. 11 and 12 the results of such a procedure are compared with the results obtained using the full spectral function (cf. Sec. IV A). It can be seen that using the Fermi motion smearing approximation yields cross sections that systematically overestimate the data for $\nu < \nu_{\text{peak}}$. On the other hand, at large values of ν in the region of inelastic channels the error is much less, although it should be remembered that for the calculation of tiny effects, such as the EMC effect, the spectral function has also to be used at $\nu > \nu_{\text{peak}}$ (cf. [13]).

D. Comparison of various off-shell and current conservation prescriptions

In this section we investigate the effects of using two of the prescriptions for treating off-shell effects and current conservation, presented in Sec. II B [prescriptions (a) and (c)]. One of the motivations for such a comparison is that, while several papers have been written in which off-shell effects are investigated in the q.e., part of nuclear cross sections (see, e.g., [30] and references therein), to our knowledge, a similar analysis has been carried out for the inelastic channels only in [20] in the case of ^{3}He. Moreover, since it has been impossible so far to treat exactly gauge invariance in electron-nucleus scattering involving a generic A-nucleon system, it is important to have a qualitative understanding of the ambiguity that one introduces in these calculations. Such information can be obtained by comparing the results of two different treatments of off-shell effects, as the ones leading to

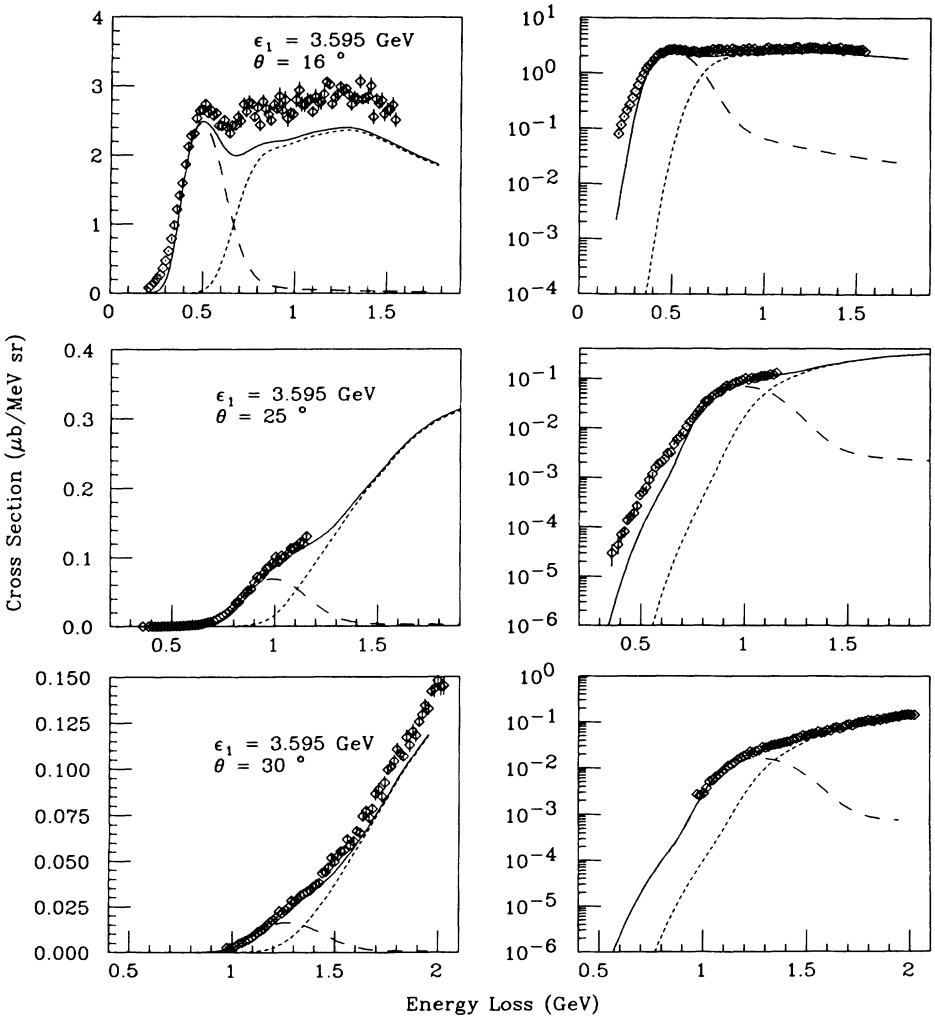

FIG. 5. The same as in Fig. 4 but for ^{12}C. Experimental data from [18].

prescriptions (a) and (c). They represent two extreme cases, as shown in Sec. II C in that in prescription (a) the components of the four momentum transfer are the same for both the nucleus and the internal nucleon, whereas in prescription (c) the energy transfer to the nucleus is assumed to be different from the one to the off-shell nucleon. It should be noted that the coefficients C_1 and D_1 [Eqs. (25)–(27)] are the same in all prescriptions, which leaves, unchanged the response W_1^A and, consequently, the transverse response R_T^A. The only difference is in the coefficients C_2 and D_2, which affect the response W_2^A, and therefore R_L^A. This reflects the way gauge invariance has been restored in all considered prescriptions (see also [20]). Since the experimental cross sections shown in this paper are mainly transverse, it is expected that the two different prescriptions should not lead to very different results. Furthermore, the larger the momentum and the energy transfers, the smaller the difference between the prescriptions [it should be pointed out in this respect that by taking exactly the Bjorken limit in Eqs. (26b) and (27b), i.e., $Q^2 \to \infty$, $\nu \to \infty$, and x fixed, any difference between the two prescriptions vanishes]. The results of our calculations are presented in Fig. 13. It can be seen that, while at $Q^2 \approx 1$ prescriptions (a) and (c) lead to a 10% difference which persists in the whole range of ν on the right side of the quasielastic (q.e.) peak, at $Q^2 \approx 3$ GeV^2 the two prescriptions yield essentially the same results.

V. THE EFFECTS OF INELASTIC CHANNELS ON THE QUASIELASTIC STRUCTURE FUNCTIONS AT $x > 1$ (y SCALING)

One of the most important aspects in the study of inclusive quasielastic scattering at $x > 1$ is the extraction of the y-scaling function from the experimental cross section. The scaling function is defined by the following quantity [2,3]:

$$F(y,|\mathbf{q}|) = \frac{\sigma_2(y,|\mathbf{q}|)}{[Z\sigma_{ep} + N\sigma_{en}]} K(y,|\mathbf{q}|) \tag{32}$$

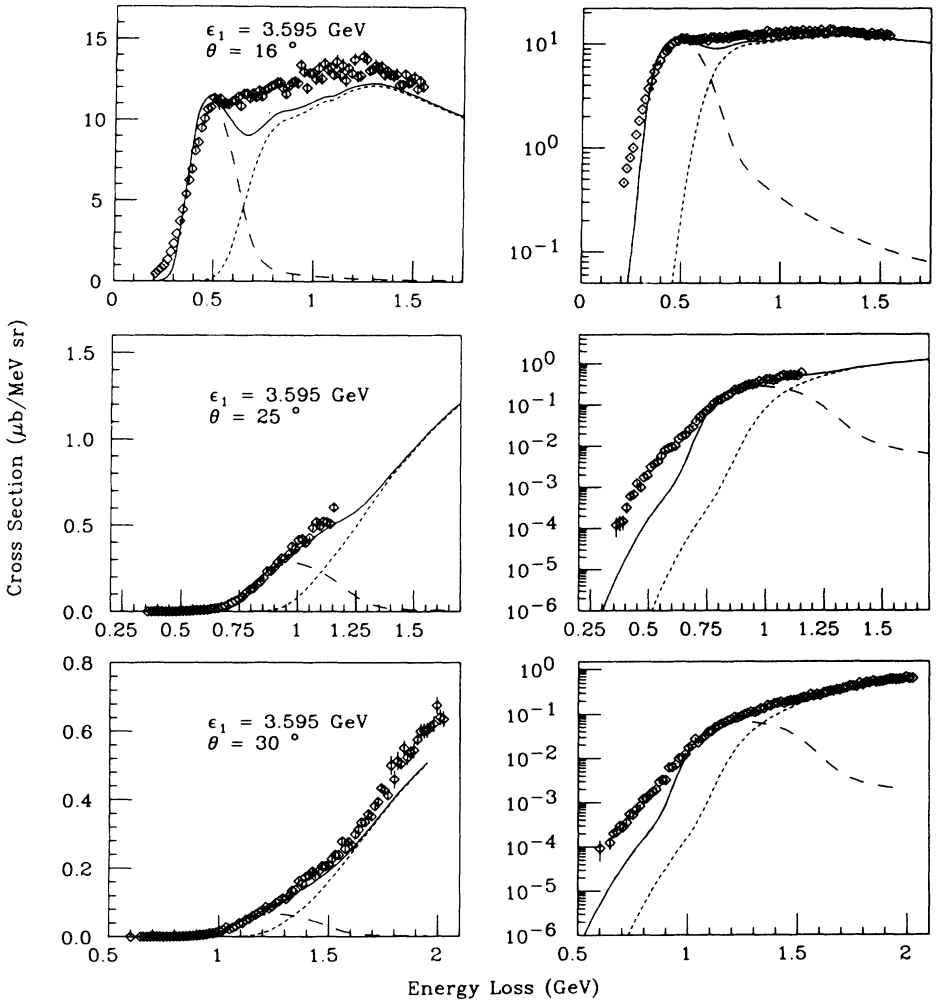

FIG. 6. The same as in Fig. 4 but for ^{56}Fe. Experimental data from [18].

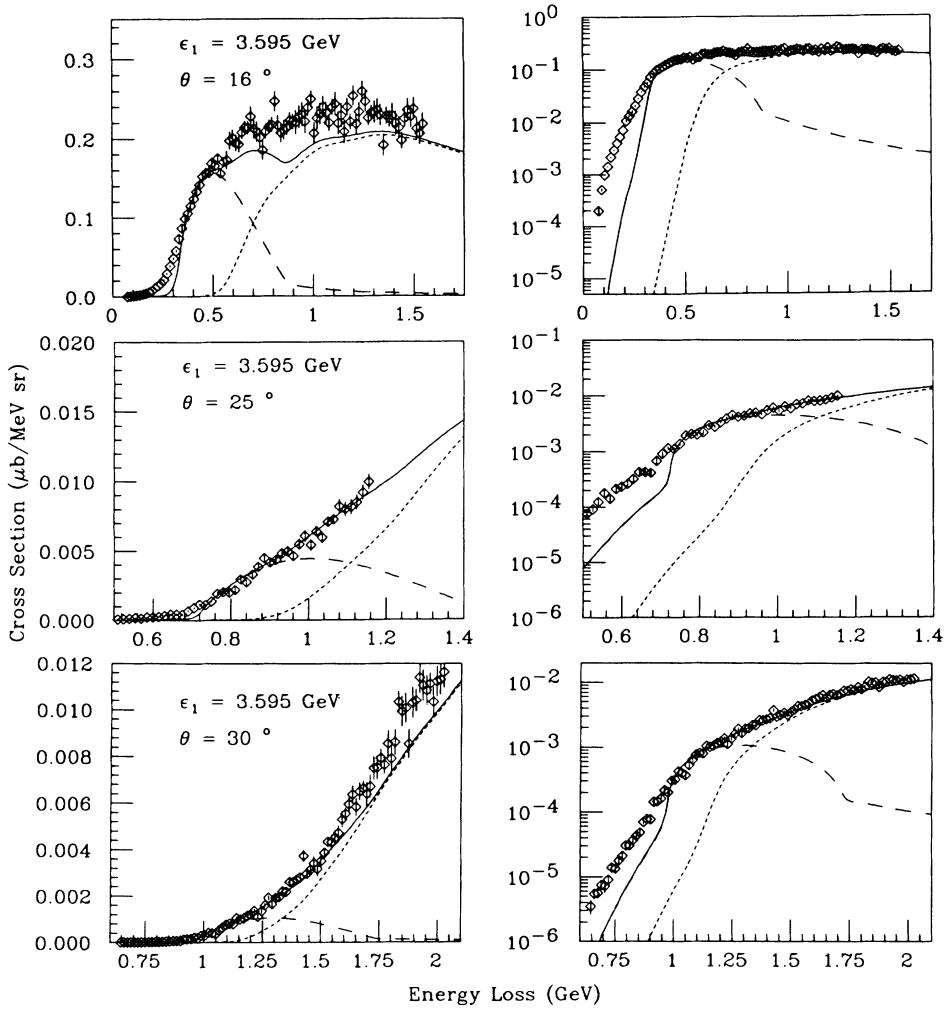

FIG. 7. The same as in Fig. 4 but for extrapolated nuclear matter. Experimental data from [19].

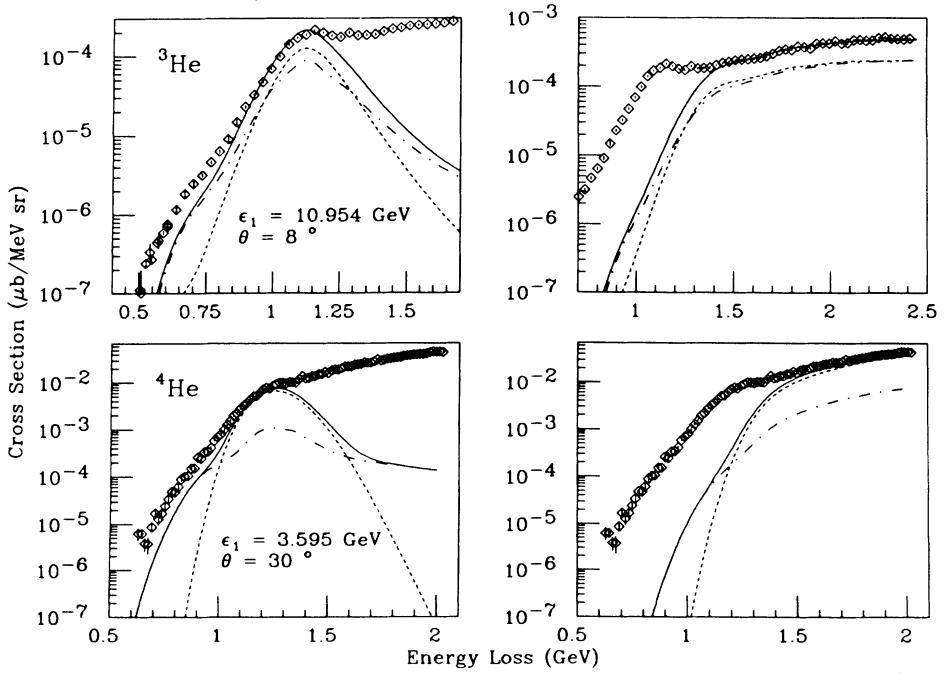

FIG. 8. The effects of nucleon-nucleon correlations on the q.e. (left) and inelastic (right) cross sections for ^{3}He and ^{4}He (solid lines). The short-dashed and dot-dashed lines represent the contribution from the uncorrelated (P_{gr}) and correlated (P_{ex}) parts of the spectral function, respectively [cf. Eq. (16)].

where $\sigma_2(y,|\mathbf{q}|)=(d^2\sigma/d\Omega d\epsilon_2)_{\text{q.e.}}$, $\sigma_{eN}\equiv d\sigma/d\Omega$ is the off-shell electron-nucleon cross section, e.g., Eq. (30), and $K(y,|\mathbf{q}|)=|\mathbf{q}|/[M_N^2+(|\mathbf{q}|+y)^2]$. The scaling variable y is given by the solution of the following equation:

$$\nu+M_A=[M_N^2+(|\mathbf{q}|+y)^2]^{1/2}+[M_{A-1}^2+y^2]^{1/2} \quad (33)$$

which represents the energy conservation corresponding to the scattering of the virtual photon by a nucleon having the minimum values of the momentum and removal energy, $|y|=k_{\min}(|\mathbf{q}|,\nu,E_{\min})$. At high momentum transfer the inclusive cross section (31), which appears in the numerator of (32), factorizes to a good approximation [2,3] and one can define the theoretical scaling function as

$$F^{\text{th}}(y,|\mathbf{q}|)=2\pi\int_{E_{\min}}^{E_{\max}(y,|\mathbf{q}|)}dE\int_{k_{\min}(y,|\mathbf{q}|,E)}^{k_{\max}(y,|\mathbf{q}|,E)}dk\,kP(k,E)\ , \quad (34)$$

where, for ease of presentation, we have defined for the present section $|\mathbf{p}|\equiv k$. In the asymptotic limit ($|\mathbf{q}|\to\infty, y$ fixed), F^{th} scales in y and becomes the asymptotic scaling function [3].

$$F^{\text{th}}(y)=2\pi\int_{E_{\min}}^{\infty}dE\int_{|y-(E-E_{\min})|}^{\infty}dk\,kP(k,E)\ . \quad (35)$$

The knowledge of the experimental asymptotic scaling function $F^{\text{exp}}(y)$ [i.e., the q-independent quantity (32) with $\sigma_2=\sigma_2^{\text{exp}}$] in the region of negative values of y would allow one to obtain the nucleon momentum distribution [3]. As a matter of fact, in [3], by using for σ_2^{exp} the same experimental data considered in this paper, the scaling function (32) has been used to obtain the asymptotic scaling function and the nucleon momentum distributions in the region $50\le k\le 600$ MeV/c. It should be pointed out, however, that the y-scaling analysis of inclusive scattering relies on the assumption that the experimental cross section to be used in (32) is totally quasielastic, without any contamination from inelastic channels. In order to check the validity of such an assumption, we have calculated the quantity (32) using, in the numerator, the quasi-

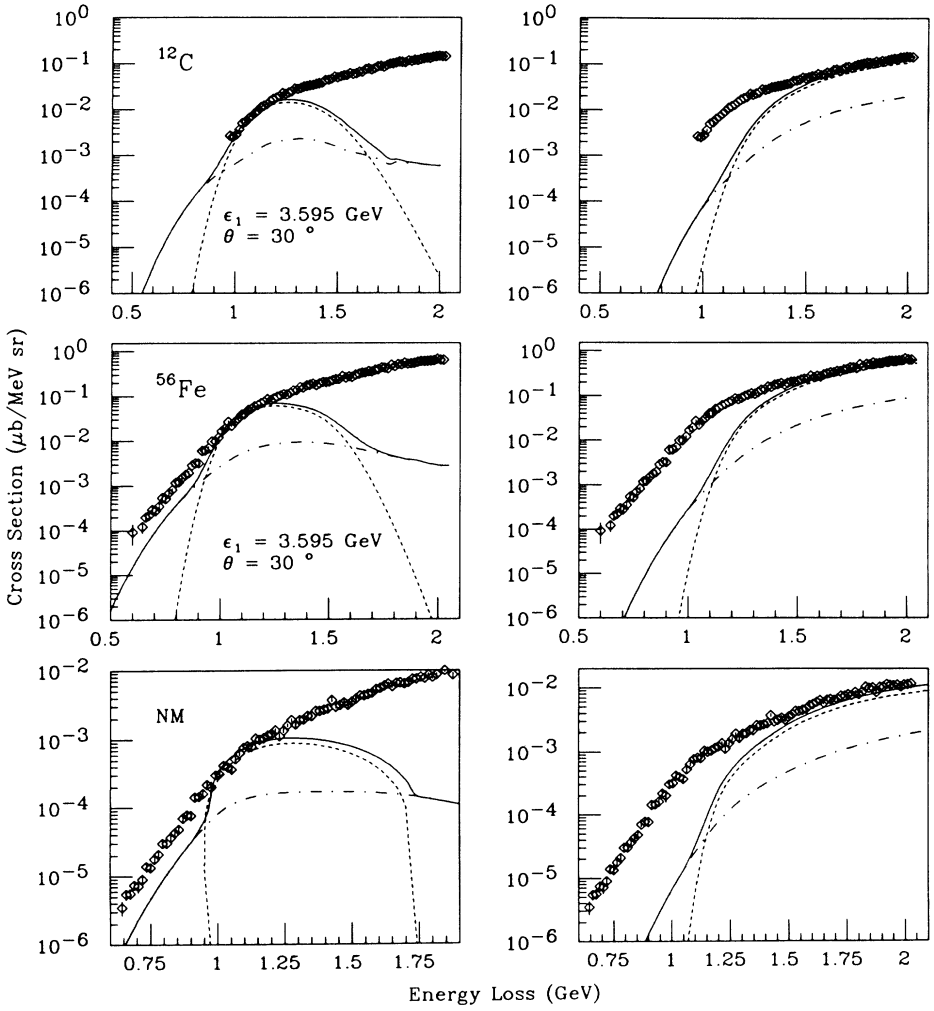

FIG. 9. The effects of nucleon-nucleon correlations on the q.e. (left) and inelastic (right) cross sections for ^{12}C, ^{56}Fe, and nuclear matter (solid lines). The short-dashed and dot-dashed lines represent the contribution from the uncorrelated (P_0) and correlated (P_1) parts of the spectral function, respectively [cf. Eq. (18)].

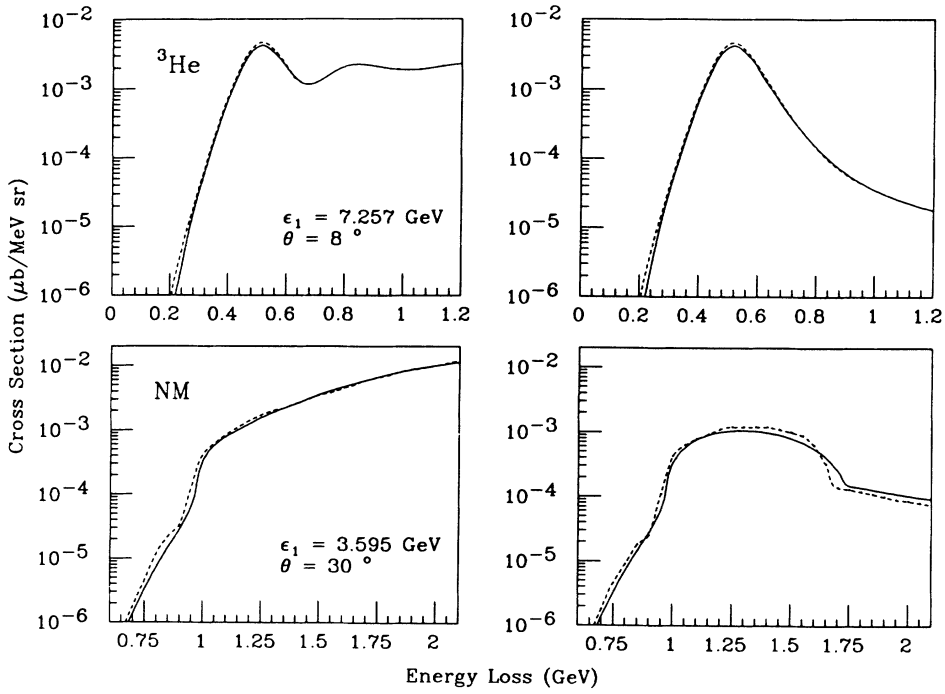

FIG. 10. Comparison of theoretical cross sections (right) and total cross sections (left) obtained with different spectral functions for ^{3}He and nuclear matter. For both nuclei the solid line corresponds to the model spectral function of [15] whereas the dashed line corresponds to the variational wave function of [7] for ^{3}He and the many-body correlated wave function of [9] for nuclear matter.

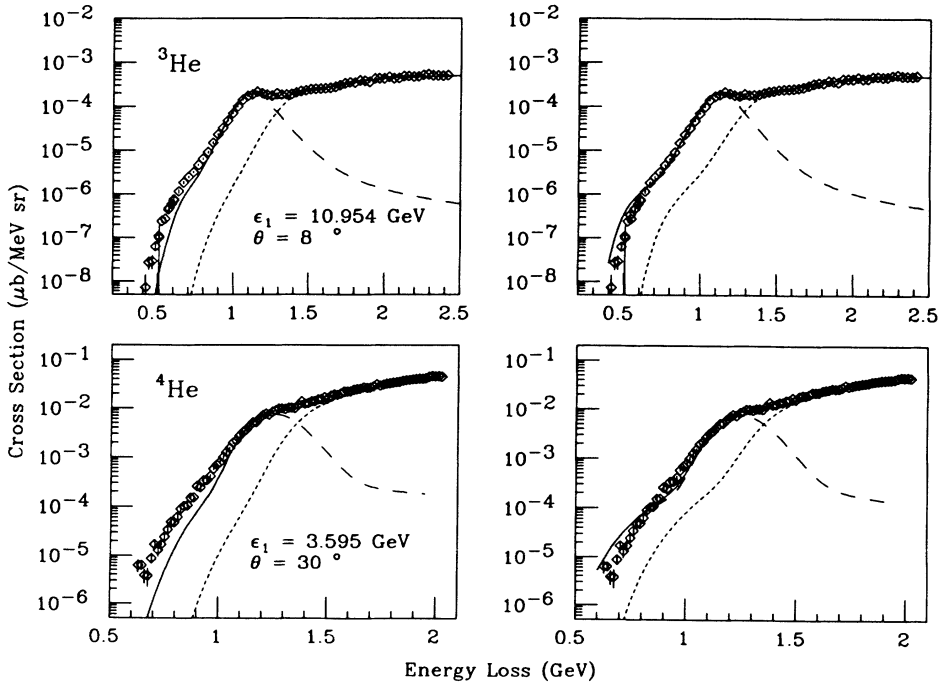

FIG. 11. Comparison of the results for ^{3}He and ^{4}He obtained with the spectral function (left) and with the Fermi smearing approximation (right).

elastic cross section as well as the sum of the quasielastic plus inelastic cross sections. The results are presented in Fig. 14 for two values of y. It can be seen that whereas at $y=0$ the effect of inelastic channels is appreciable at $Q^2 \geq 3$ GeV^2, for negative values of y the contribution of the inelastic channels to the scaling function becomes non-negligible only for values of $Q^2 \geq 8$ GeV^2. It can be concluded therefore, that present experimental data up to $Q^2 \approx 3$ GeV^2 are quasielastic in nature and can therefore be used to extract the y-scaling function and the momentum distributions as in [3].

VI. THE DEEP INELASTIC STRUCTURE FUNCTION AT $x > 1$

Deep inelastic scattering at $x > 1$ is very sensitive to nuclear structure effects and to possible variations of the quarks' momentum distributions inside the nuclear medium, since in this region the struck quark is carrying a momentum fraction greater than that available in a free nucleon [5]. Several calculations have shown in particular that the structure function $F_2^A(x,Q^2)=\nu W_2^A(x,Q^2)$ at $x > 1$ reflects very sharply the momentum and energy distributions of the spectral function [5,31,32,33], as well as the presence of exotic configurations (e.g., 6- and 9-quark bags) in the nuclear wave function [34]. Experimental data in the region $1 \leq x \leq 2$ in the Bjorken limit would be therefore very effective in probing NN correlations as well as different models of exotic configurations in nuclei. As it appears from the results presented in the previous sections, at $x > 1$ the inclusive cross section at moderate Q^2 is dominated by quasielastic scattering. It is clear therefore that, in order to extract the deep inelastic structure functions, experimental data at momentum transfers much higher than that presently available are necessary. This is illustrated in Fig. 15, where the ratio of the quasielastic cross section to the sum of the quasielastic plus in-

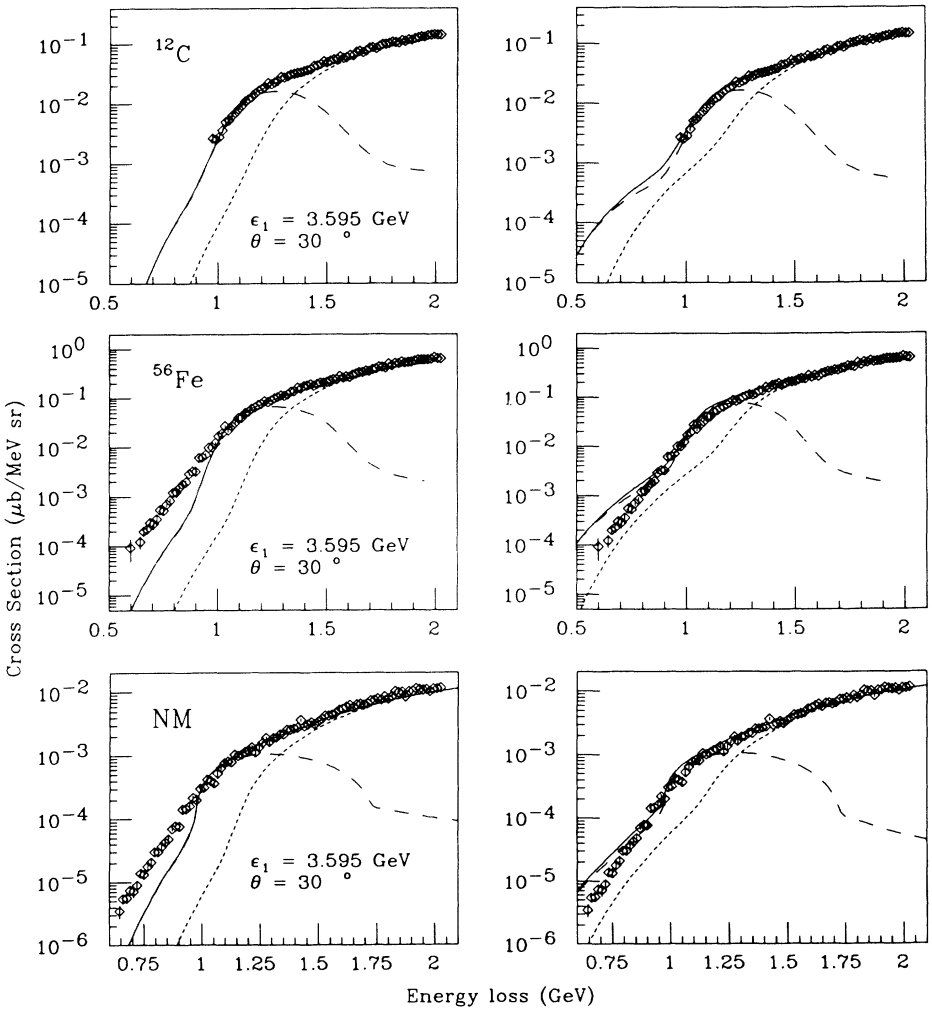

FIG. 12. The same as in Fig. 11 but for ^{12}C, ^{56}Fe, and nuclear matter.

elastic cross sections is shown for the values $x=1$ and $x=1.5$ in ^{56}Fe. Calculations have been performed both within the Fermi smearing approximation and using the correct smearing with the spectral function (the results for other nuclei are very similar to the ones for ^{56}Fe). The following remarks are in order.

(i) At $x=1$ the inclusive cross section is dominated by the inelastic channels as Q^2 increases, whereas at $x=1.5$ the quasielastic channel still strongly contributes even at the highest values of Q^2.

(ii) The results obtained within the Fermi smearing approximation appreciably differ from the ones obtained with the full spectra function, which is in line with the observation [32,31] that binding effects are particularly important at $x>1$. (iii) A thorough analysis [33] of the optimal kinematic conditions which are necessary to extract the DIS structure function from inclusive cross sections shows that a high current (100 μA) and high energy ($\approx$20 GeV) electron beam is a prerequisite.

VII. SUMMARY AND CONCLUSIONS

In this paper inclusive electron scattering by nuclei ranging from ^{3}He up to nuclear matter has been analyzed within the PWIA. Nuclear structure effects have been considered by using a spectral function which contains momentum and removal energy dependences generated by *NN* correlations, and various prescriptions to extrapolate off-shell the free electron-nucleon cross section were also studied. The results obtained exhibit many common features through the periodic table, the most important ones being as follows.

(i) The quasielastic cross section is fairly well reproduced in the region of the peak ($x\approx1$) whereas it is

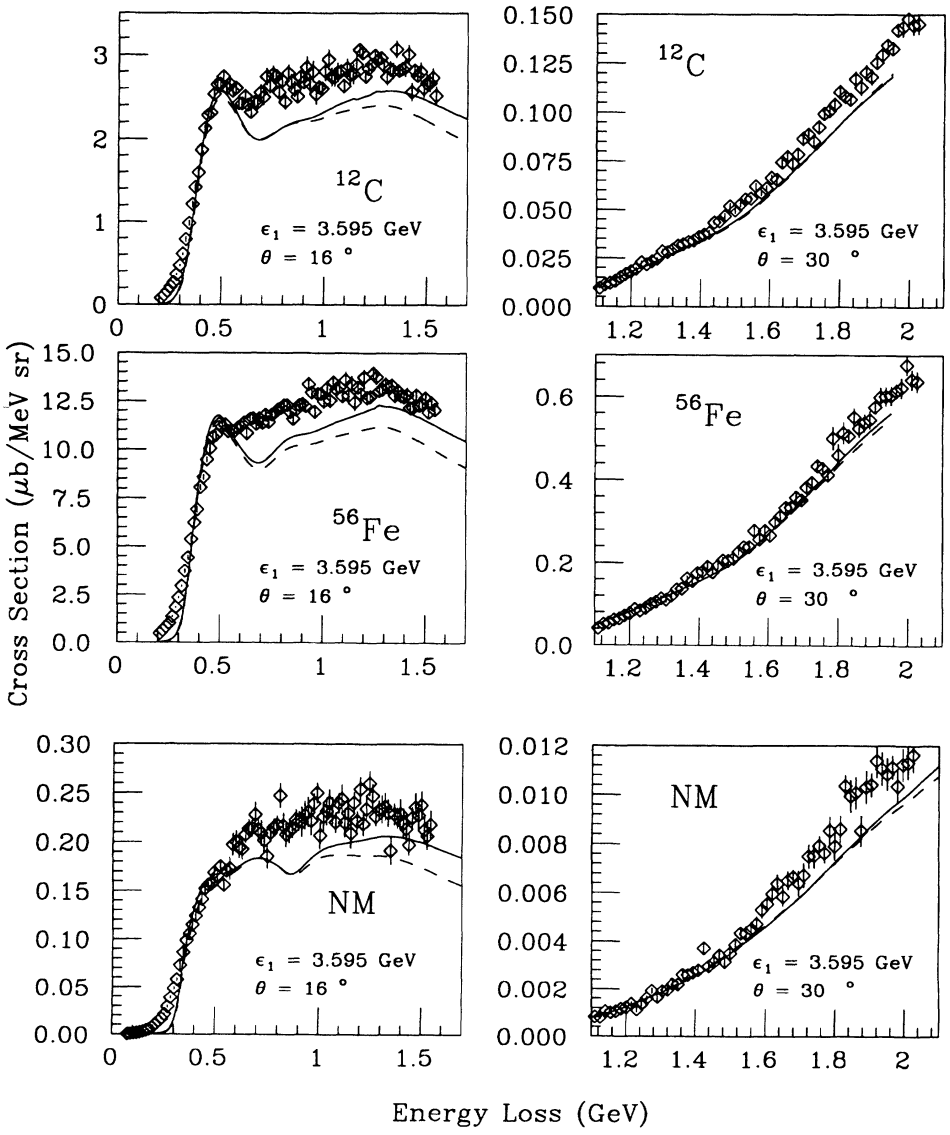

FIG. 13. Comparison of results obtained for ^{12}C, ^{56}Fe, and nuclear matter with different off-shell prescriptions. Solid line: prescription (a); dashed line: prescription (c).

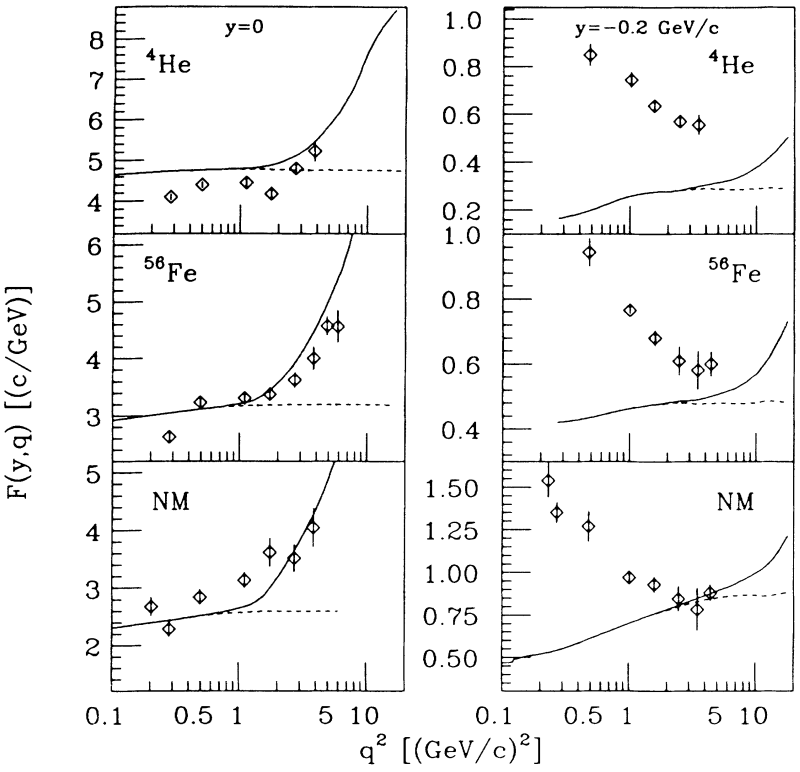

FIG. 14. The function $F(y,|\mathbf{q}|)$ [Eq. (32)] in ^{56}Fe, plotted vs the square of the three-momentum transfer for two different values of y: $y=0$ (left) and $y=-0.2$ GeV/c (right). The theoretical function, $F^{\text{th}}(y,|\mathbf{q}|)$ [Eq. (34)], is compared with the experimental quantity obtained in [3] from the inclusive data of [18,19]. The solid lines include the contribution of both the q.e. and inelastic channels, whereas the dashed lines show the contribution of the q.e. part only.

strongly underestimated in the region at $x>1$, which is dominated by the effects of nucleon-nucleon correlations. Various calculations, using different approaches [3,21,28,29], show that final-state interactions appreciably affects the cross section at $x>1$ ($y<0$). A systematic calculation of FSI effects on the cross sections considered in the present paper is underway and will be reported elsewhere. (ii) Except for the data at lower momentum transfer, where the "dip" region is appreciably underestimated, the inelastic and deep inelastic cross sections are fairly well reproduced. (iii) The Fermi smearing approximation strongly overestimates the quasielastic and inelastic cross sections at $x\geq 1$ (even by an order of magnitude at large x). (iv) The effects due to the ambiguities related to the off-shell extrapolation of the electron-nucleon cross section and to the restoration of gauge invariance are not relevant to the experimental data we have considered, and become negligible at high momentum transfer.

(v) Our calculations show that the effects of inelastic channels at $x>1$ ($y<0$) is of minor role; this means, on one side, that the existing data can be safely analyzed in terms of y scaling and, on the other side, that they cannot be used to extract the DIS structure function; to this end, as already pointed out, a high energy (20 GeV) and high luminosity electron beam would be necessary.

ACKNOWLEDGMENTS

This work was supported in part by the Department of Energy, the National Science Foundation, and the Institute of Nuclear and Particle Physics at the University of Virginia. One of us (S.L.) would also like to thank the nuclear physics group at the University of Virginia for support and warm hospitality during her visits.

APPENDIX A: THE INCLUSIVE CROSS SECTION IN FIRST BORN APPROXIMATION

The inclusive cross section for electron scattering by nuclei is

$$\frac{d^2\sigma}{d\Omega_{e'}d\epsilon_2}=\frac{\alpha^2}{Q^4}L_{\mu\nu}W^A_{\mu\nu} \tag{A1}$$

with the leptonic and hadronic tensor given by

$$L_{\mu\nu}=k_{1\mu}k_{2\nu}+k_{2\mu}k_{1\nu}-\frac{Q^2}{2}g_{\mu\nu} \tag{A2}$$

and

$$W^A_{\mu\nu}=(2\pi)^4\overline{\sum_{\alpha_A}}\sum_{\alpha_{X,f}}\int d\mathbf{P}_X\langle P_A,\alpha_A|J^A_\mu(0)|P^f_X,\alpha_X\rangle\langle P^f_X,\alpha_X|J^A_\nu(0)|P_A,\alpha_A\rangle\delta^4(P_A-P_X-q)\,, \tag{A3}$$

respectively. In Eqs. (A1) and (A3), $k_{1(2)}\equiv(\mathbf{p}_{1(2)},\epsilon_{1(2)})$ represents the initial (final) electron four-momentum, $q\equiv(\nu,\mathbf{q})\equiv k_1-k_2$ $(Q^2=-q^2=\mathbf{q}^2-\nu^2)$ the four-momentum transfer, and $P_A\equiv(M_A,0)$ the four-momentum of the initial nucleus in the laboratory system; $|P^f_X,\alpha_X\rangle$ denotes the final hadronic state X, with

c.m. four-momentum P_X and spin α_X. As is well known, the general structure of $W^A_{\mu\nu}$ which satisfies time-reversal invariance and parity and gauge conservation is

$$W^A_{\mu\nu} = -\left[g_{\mu\nu} + \frac{q_\mu q_\nu}{Q^2}\right] W_1^A(Q^2,W) + \left[P_{A\mu} + \frac{(P_A q)}{Q^2} q_\mu\right]\left[P_{A\nu} + \frac{(P_A q)}{Q^2} q_\nu\right] \times \frac{W_2^A(Q^2,W)}{M_A^2} . \quad \text{(A4)}$$

By contracting the leptonic and hadronic tensors, one obtains the well known formula for the inclusive cross section

$$\frac{d^2\sigma}{d\Omega d\epsilon_2} = \sigma_{\text{Mott}}[W_2^A(Q^2,W) + 2\tan^2\frac{\theta}{2} W_1^A(Q^2,W)] . \quad \text{(A5)}$$

APPENDIX B: THE CROSS SECTION IN PLANE WAVE IMPULSE APPROXIMATION

In order to evaluate Eq. (1) within microscopic nuclear structure, certain assumptions have to be done at the level of the matrix element of the hadronic current $\langle P_A,\alpha_A|J^A_\mu(0)|P^f_X,\alpha_X\rangle$. In this paper we shall consider the nonrelativistic PWIA based on the following assumptions: (1) The states $|P,\alpha\rangle$ are eigenfunctions of the nonrelativistic many-body Hamiltonian. (2) The current operator J^A_ν is a sum of single-nucleon operators,

$$J^A_\nu = \sum_{N=1}^{A} j^N_\nu . \quad \text{(B1)}$$

(3) The target virtually decays into a onshell $(A-1)$-nucleon system (in either the ground or excited states) and an off-shell nucleon. (4) The virtual photon interacts with the off-shell nucleon and a hadronic state is created, which leaves the target without interacting [with eigenfunctions Ψ^0_A and Ψ^f_{A-1}, respectively, corresponding to the ground state of the A-particle Hamiltonian $\hat{H}_A$ and to the state f of the $(A-1)$-particle Hamiltonian $\hat{H}_{A-1}$] with the spectator $(A-1)$-nuclear system; this means that the final hadronic state $|P^f_X,\alpha_X\rangle$ has the following form [for notations cf. Fig. 2 and Eqs. (5)–(8)]:

$$|P^f_X,\alpha_X\rangle = \mathcal{A}\{|\phi_X,\mathbf{p}_X\rangle|\Psi^f_{A-1},-\mathbf{p}\rangle\} \quad \text{(B2)}$$

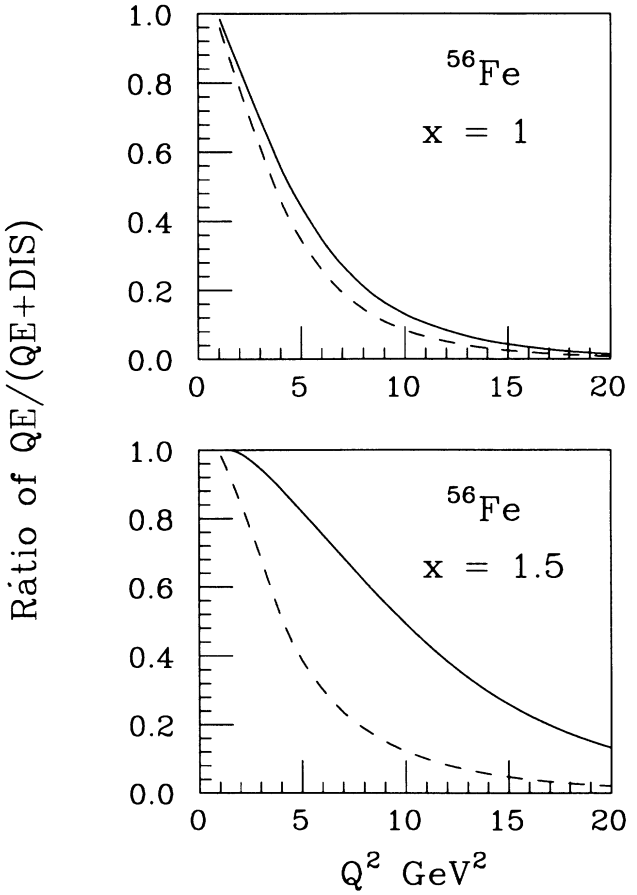

FIG. 15. Ratio between the q.e. contribution to the (e,e') cross section for ^{56}Fe and the total cross section (q.e. plus inelastic), plotted vs Q^2 at two different values of Bjorken x: $x=1$ (top), $x=1.5$ (bottom). The solid lines were obtained by using the spectral function of [14], whereas the dashed lines correspond to the Fermi smearing approximation. It can be seen that, at larger values of x, the two calculations yield sensibly different results in the high-Q^2 region.

where $\mathcal{A}$ is a Pauli antisymmetrizer. Within the above assumptions, the hadronic tensor takes the form

$$W^A_{\mu\nu} = \int d\mathbf{p} \int dE [ZP^p(|\mathbf{p}|,E) W^{p,\text{off}}_{\mu\nu}(p,q) + NP^n(|\mathbf{p}|,E) W^{n,\text{off}}_{\mu\nu}(p,q)] , \quad \text{(B3)}$$

where $P^N(|\mathbf{p}|,E)$ $(N=p,n)$ is the nucleon spectral function

$$P^N(|\mathbf{p}|,E) = \langle \Psi^0_A | a^\dagger_{\mathbf{p}} \delta(E-(\hat{H}_{A-1}-E_A)) a_{\mathbf{p}} | \Psi^0_A \rangle \quad \text{(B4)}$$

$$= \sum_f |\langle \phi_{\mathbf{p}}, \Psi^f_{A-1} | \Psi^0_A \rangle|^2 \delta(E-(E^f_{A-1}-E_A)) \quad \text{(B5)}$$

representing the joint probability of finding in a nucleus a nucleon with momentum $\mathbf{p}$ and removal energy $E=E^f_{A-1}-E_A=E_{\min}+E^{f*}_{A-1}$, with $E_{\min}=|E_A|-|E_{A-1}|=M_N+M_{A-1}-M_A$, where $E^f_{A-1}=E_{A-1}+E^{f*}_{A-1}$ and E_A are the eigenvalues (with eigenfunctions Ψ^0_A and Ψ^f_{A-1}, respectively) corresponding to the ground state of the A-particle Hamiltonian $\hat{H}_A$, and to the state f of the $(A-1)$-particle Hamiltonian $\hat{H}_{A-1}$, E^{f*}_{A-1} being the intrinsic excitation energy. In Eq. (B3) $W^{p,\text{off}}_{\mu\nu}$ is the hadronic tensor for an off-shell proton (neutron) whose form is in principle un-

known; a generally adopted approach is to assume that $W_{\mu\nu}^{p(n),\text{off}}$ has the same form as the one for a free nucleon, i.e.,

$$W_{\mu\nu}^{p(n)} = -\left[g_{\mu\nu}+\frac{q_\mu q_\nu}{Q^2}\right]W_1^{p(n)}(Q^2,W)+s_\mu s_\nu\frac{W_2^{p(n)}}{M_N^2}(Q^2,W)\ ,$$
$$s_\mu = \left[p_\mu+\frac{(pq)}{Q^2}q_\mu\right]\ . \tag{B6}$$

Making several assumptions about the off-shell continuation of the different quantities which appear in Eq. (B5), we obtain

$$W_{\mu\nu}^{p(n),\text{off}} = -\left[g_{\mu\nu}+\frac{\tilde{q}_\mu\tilde{q}_\nu}{\tilde{Q}^2}\right]W_1^{p(n),\text{off}}(\tilde{Q}^2,\tilde{W},p^2)+\tilde{s}_\mu\tilde{s}_\nu\frac{W_2^{p(n),\text{off}}}{M_N^2}(\tilde{Q}^2,\tilde{W},p^2)\ ,$$
$$\tilde{s} = \left[p_\mu+\frac{(p\tilde{q})}{\tilde{Q}^2}\tilde{q}_\mu\right]\ , \tag{B7}$$

where all kinematic variables have to be evaluated within the given off-shell prescription. Inserting Eq. (B7) in Eq. (B3) and using Eq. (A4), it is a usual procedure to obtain the explicit form of $W_{1(2)}^A(Q^2,W)$ as a convolution integral involving the nucleon spectral function and $W_{1,2}^{p(n),\text{off}}(\tilde{Q}^2,\tilde{W},p^2)$. It should be pointed out that because of off-shell effects $q_\mu W_{\mu\nu}^{p(n),\text{off}} = W_{\mu\nu}^{p(n),\text{off}} q_\nu \neq 0$ and $q_\mu W_{\mu\nu}^A = W_{\mu\nu}^A q_\nu \neq 0$ so that current conservation is violated. Two strategies are followed at this point: either the problem of current conservation is completely disregarded or gauge invariance is restored by *ad hoc* procedures; the usual one is to keep some of the components of $W_2^{p(n),\text{off}}$ as given by Eq. (B7) (e.g., the transverse and time ones as in [11]) and to constrain the form of the other components (e.g., the longitudinal ones, [11]) by enforcing the continuity equation $q_\mu W_{\mu\nu}^{p(n),\text{off}} = W_{\mu\nu}^{p(n),\text{off}} q_\nu = 0$. Different choices for the off-shell kinematic variables and for the restoration of current conservation will result in different forms for the convolution integral for $W_{1(2)}^A$. The general form can be written as

$$W_{1(2)}^A(Q^2,W) = \int d\mathbf{p}\int dE\, ZP^p(|\mathbf{p}|,E)[C_{1(2)}W_1^{p,\text{off}}(\tilde{Q}^2,\tilde{W},p^2)+D_{1(2)}W_2^{p,\text{off}}(\tilde{Q}^2,\tilde{W},p^2)]+(\text{similar terms for neutrons}) \tag{B8}$$

where the dependence on the off-shell choice is incorporated in the coefficients $C_{1(2)}$ and $D_{1(2)}$.

[1] B. Frois and C. Papanicolas, Annu. Rev. Nucl. Part. Sci. **37**, 133 (1987); D. Drechsel and M. M. Giannini, Rep. Prog. Phys. **52**, 1083 (1989).
[2] D. B. Day, J. S. McCarthy, T. W. Donnelly, and I. Sick, Annu. Rev. Nucl. Part. Sci. **40**, 357 (1990).
[3] C. Ciofi degli Atti, E. Pace and G. Salmé, Phys. Rev. C **43**, 1155 (1991), and references therein.
[4] E. L. Berger and F. Coester, Annu. Rev. Nucl. Part. Sci. **37**, 463 (1987).
[5] L. L. Frankfurt and M. I. Strikman, Phys. Rep. **160**, 235 (1988).
[6] H. Meier-Hajduk, Ch. Hadjuk, P. U. Sauer, and W. Theis, Nucl. Phys. **A395**, 332 (1983).
[7] C. Ciofi degli Atti, E. Pace, and G. Salmé, Phys. Rev. C **21**, 805 (1980); Phys. Lett. **127B**, 303 (1983).
[8] A. E. L. Dieperink, T. de Forest, I. Sick, and R. A. Brandenburg, Phys. Lett. **63B**, 261 (1976).
[9] O. Benhar, A. Fabrocini, and S. Fantoni, Nucl. Phys. **A505**, 267 (1989).
[10] A. Bodek and J. L. Ritchie, Phys. Rev. D **23**, 1070 (1981).
[11] T. de Forest, Nucl. Phys. **A392**, 232 (1982).
[12] C. Ciofi degli Atti, Prog. Part. Nucl. Phys. **3**, 163 (1980), and references therein.
[13] C. Ciofi degli Atti and S. Liuti, Phys. Lett. **225B**, 215 (1988).
[14] C. Ciofi degli Atti, S. Liuti, and S. Simula, Phys. Rev. C **14**, R2474 (1990).
[15] C. Ciofi degli Atti, S. Simula, L. L. Frankfurt, and M. I. Strikman, in *4th Workshop on Perspectives in Nuclear Physics at Intermediate Energies,* edited by S. Boffi, C. Ciofi degli Atti, and M. M. Giannini (World Scientific, Singapore, 1989, p. 312; Phys. Rev. C **43**, (1991).
[16] S. Galster *et al.*, Nucl. Phys. **B32**, 221 (1971).
[17] D. B. Day *et al.*, Phys. Rev. Lett. **43**, 1143 (1979).
[18] D. B. Day *et al.*, Phys. Rev. Lett. **59**, 427 (1987).
[19] D. B. Day *et al.*, Phys. Rev. C **40**, 1011 (1989); D. H. Potterveld, Ph.D. thesis, Caltech, 1989, unpublished.
[20] H. Meier-Hajduk, U. Oelfke, and P. U. Sauer, Nucl. Phys. **A499**, 637 (1989).
[21] O. Benhar, A. Fabrocini, S. Fantoni, G. A. Miller, V. R. Pandharipande, and I. Sick, Phys. Rev. C **44**, 2328 (1991).
[22] Y. Akaishi, Nucl. Phys. **A416**, 409c (1984).
[23] R. Schiavilla, V. R. Pandharipande, and R. B. Wiringa, Nucl. Phys. **A449**, 219 (1986).
[24] O. Benhar, C. Ciofi degli Atti, S. Liuti, and G. Salmé, Phys. Lett. B **177**, 135 (1986).
[25] Xiandong Ji and J. Engel, Phys. Rev. C **40**, R497 (1989).
[26] S. Frullani and J. Mougey, in *Advances in Nuclear Physics,* edited by J. W. Negele and E. Vogt (Plenum, New York, 1984), Vol. 14, p. 1.
[27] C. Ciofi degli Atti, E. Pace, and G. Salmé, Phys. Rev. C **36**, 1208 (1987).
[28] J. M. Laget, Phys. Lett. **151B**, 325 (1985).
[29] R. Cenni, C. Ciofi degli Atti, and G. Salmé C **39**, 1425

(1989).
[30] C. R. Chinn and A. Picklesimer, Lawrence Livermore National Laboratory Report No. UCRL-JC-107072.
[31] J. Rozynek and M. C. Birse, Phys. Rev. C **38**, 2201 (1989).
[32] C. Ciofi degli Atti and S. Liuti, Phys. Rev. C **41**, 1100 (1990).
[33] D. B. Day, Nucl. Phys. **A532**, 255c (1991).
[34] H. Pirner and J. Vary, Phys. Rev. Lett. **46**, 1376 (1981).

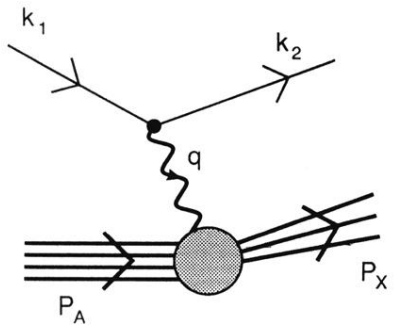

FIG. 1. Inclusive electron-nucleus scattering diagram in the one photon-exchange approximation. $k_{1(2)} \equiv (\mathbf{p}_{1(2)}, \epsilon_{1(2)})$ represents the initial (final) electron four-momentum, $q \equiv (\nu, \mathbf{q}) \equiv k_1 - k_2$ $(Q^2 = -q^2 = \mathbf{q}^2 - \nu^2)$, the four-momentum transfer, and $P_A \equiv (M_A, 0)$ and P_X the four-momenta of the initial and final nuclear systems, respectively.

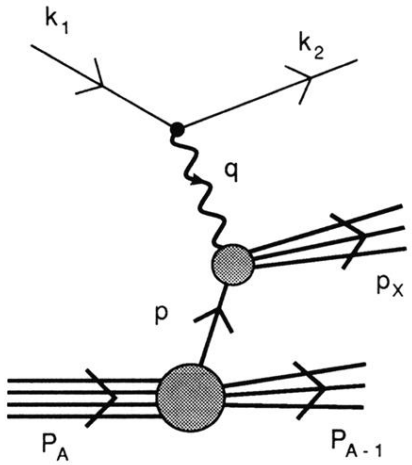

FIG. 2. Impulse approximation diagram for electron scattering off nuclei. The four-momenta in the laboratory system are $P_A \equiv (M_A, 0)$, $P_{A-1} \equiv ((\mathbf{p}^2 + M^{*2}_{A-1})^{1/2}, -\mathbf{p})$, $p \equiv (M_A - (\mathbf{p}^2 + M^{*2}_{A-1})^{1/2}, \mathbf{p})$, and $p_X \equiv ((\mathbf{p}_X^2 + M_X^2)^{1/2}, \mathbf{p}_X)$ and refer to the initial nucleus A, to the recoiling final $A-1$ system, to the struck nucleon, and to the final hadronic system at the nucleon vertex, respectively.